# Supplementary Information for

# Reverse Water-gas Shift Catalyzed by $Rh_nVO_{3,4}^-$ ($n$ = 3–7) Cluster Anions under Variable Temperatures

An Zhao,[a,c] Qing-Yu Liu,[a,d] Zi-Yu Li,[a,d] Xiao-Na Li,*[b] Sheng-Gui He*[a,c,d]

[a] State Key Laboratory for Structural Chemistry of Unstable and Stable Species, Institute of Chemistry, Chinese Academy of Sciences, Beijing 100190, China

[b] Key Laboratory of Cluster Science of Ministry of Education, School of Chemistry and Chemical Engineering, Beijing Institute of Technology, Beijing 102488, P. R. China

[c] University of Chinese Academy of Sciences, Beijing 100049, P. R. China

[d] Beijing National Laboratory for Molecular Sciences and CAS Research/Education Center of Excellence in Molecular Sciences, Beijing 100190, China

Corresponding Authors:

* Xiao-Na Li: xiaonali@bit.edu.cn; Sheng-Gui He: shengguihe@iccas.ac.cn

**Table of Contents**

# 1. Methods

## 1.1 Experimental methods

The experiments performed in this study were conducted with a reflectron time-of-flight mass spectrometer (TOF-MS) coupled with a laser ablation and supersonic expansion cluster source, a quadrupole mass filter, and a high-temperature linear ion trap (LIT) reactor. Detailed design of these apparatus can be found in our previous studies.[1-6] A brief outline of the experiments is given below. The $Rh_nVO_{3,4}^-$ ($n$ = 3−7) cluster anions were generated by laser ablation ($Nd^{3+}$: YAG, λ = 532 nm, 15−20 mJ $pulse^{-1}$, 10 Hz; Continuum Minilite laser system) of a rotating and translating mixed-metal disk compressed with Rh and V powders (molar ratio Rh/V = 5/1) in the presence of 0.05% $O_2$ seeded in the He carrier gas (99.999%) with a backing pressure of about 5.0 standard atmosphere. The considered $Rh_nVO_3^-$ and $Rh_nVO_4^-$ clusters were mass-selected using a quadrupole mass filter[5] and then entered into a high-temperature LIT reactor[6,7] where they were confined and heated to a controlled temperature by collisions with a pulse of buffer gas (He) and then interacted with another pulse of pure (or diluted) $CO_2$ and $H_2$, respectively. The high-temperature LIT reactor was formed by a set of hexapole rods and two cap electrodes that were heated using a resistive heater. The temperature was monitored using a thermocouple positioned in the LIT holder. The cluster ions ejected from the LIT were detected using a reflectron TOF-MS,[2] which was used to measure the masses and the abundance of the reactant and product ions.

## 1.2 Theoretical methods

The density functional theory (DFT) calculations at the Tao–Perdew–Staroverov–Scuseria (TPSS)[8] level using the Gaussian 09 program package[9] were carried out to investigate the structures of the $Rh_nVO_{3,4}^-$ ($n$ = 3−7) clusters as well as the mechanism for the reaction of $Rh_6VO_3^-$ with $CO_2$. The TZVP[10] basis sets for H, C, and O atoms and the Stuttgart/Dresden relativistic effective core potentials[11] (denoted as SDD in Gaussian software) for Rh atom were used. A Fortran code based genetic algorithm[12] was used to search global minimum structure of $Rh_nVO_{3,4}^-$ ($n$ = 3−7). The relaxed potential energy surface scans were used extensively to obtain the initial structures of reaction intermediates (Is) and transition states (TSs) along the pathways. Vibrational frequency calculations were carried out to check that the Is and TSs have zero and only one imaginary frequency, respectively. The TSs were optimized by using the Berny algorithm method[13] and then verified to connect two appropriate local minima by performing intrinsic reaction coordinate calculations.[14] The

zero-point vibration-corrected energies ($\Delta H_0$) in units of eV were reported in this work. A natural bond orbital (NBO) analysis was performed by using NBO 5.9.[15]

## 2. Additional studies on cluster reactivity

### 2.1 Mass spectra for the reactions of mass-selected $Rh_nVO_3^-$ ($n$ = 3–7) clusters with $CO_2$ at variable temperatures (298 – 773K)

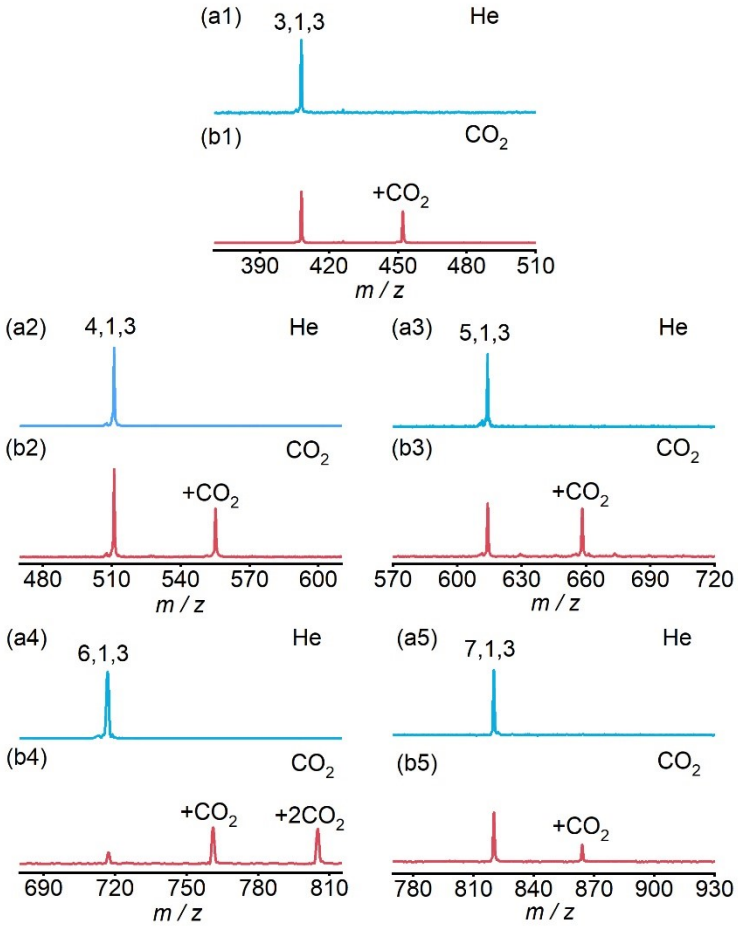


**Fig. S1** The time-of-flight (TOF) mass spectra for the reactions of mass-selected $Rh_nVO_3^-$ ($n$ = 3–7) clusters (a) with $CO_2$ (b) at 298K. The average molecule density of reactant gas is about $3 \times 10^{12}$ (b1), $13\times 10^{12}$ (b2), $13 \times 10^{12}$ (b3), $129 \times 10^{12}$ (b4), and $5 \times 10^{12}$ molecule per $cm^3$ (b5). The reaction times are about 1.8 ms for $Rh_3VO_3^- + CO_2$, 1.9 ms for $Rh_{4,5}VO_3^- + CO_2$, and 2.1ms for $Rh_{6,7}VO_3^- + CO_2$. The $Rh_xV_yO_z^-$ and $Rh_xV_yO_zX^-$ species (X = $CO_2$ and $2CO_2$) are labeled as $x$,$y$,$z$ and +X, respectively.

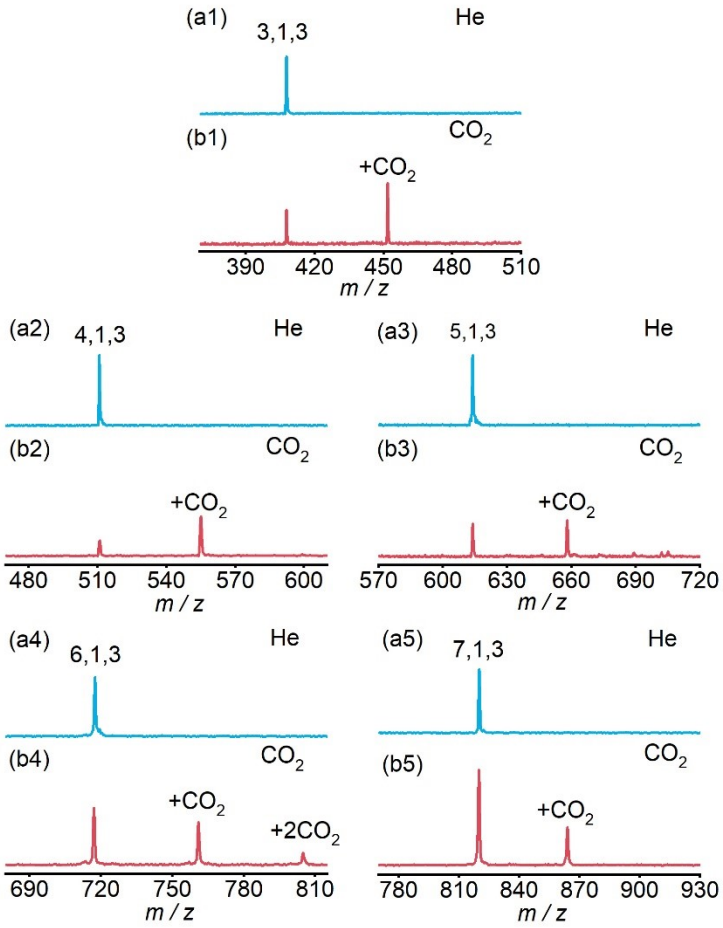


**Fig. S2** The TOF mass spectra for the reactions mass-selected $Rh_nVO_3^-$ ($n$ = 3–7) clusters (a) with $CO_2$ (b) at 373 K. The average molecule density of reactant gas is about $8 \times 10^{12}$ (b1), $75\times 10^{12}$ (b2), $39 \times 10^{12}$ (b3), $154 \times 10^{12}$ (b4), and $8 \times 10^{12}$ molecule per $cm^3$ (b5). The reaction times are about 1.7 ms for $Rh_{3,4}VO_3^-$ + $CO_2$ and 2.1 ms for $Rh_{5\text{-}7}VO_3^-$ + $CO_2$. The $Rh_xV_yO_z^-$ and $Rh_xV_yO_zX^-$ species (X = $CO_2$ and $2CO_2$) are labeled as $x$,$y$,$z$ and +X, respectively.

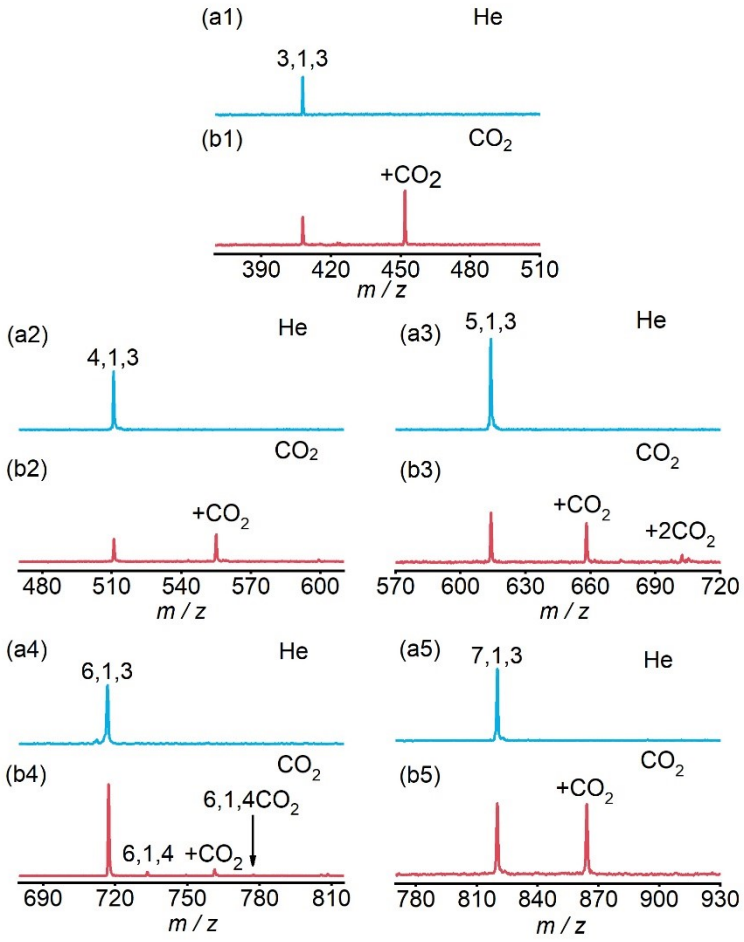


**Fig. S3** The TOF mass spectra for the reactions of mass-selected $Rh_nVO_3^-$ ($n$ = 3–7) clusters (a) with $CO_2$ (b) at 473 K. The average molecule density of reactant gas is about 12 × $10^{12}$ (b1), 110× $10^{12}$ (b2), 67 × $10^{12}$ (b3), 48 × $10^{12}$ (b4), and 22 × $10^{12}$ molecule per $cm^3$ (b5). The reaction times are about 2.1 ms for $Rh_{3,4}VO_3^-$ + $CO_2$ and 22 ms for $Rh_{5\text{-}7}VO_3^-$ + $CO_2$. The $Rh_xV_yO_z^-$ and $Rh_xV_yO_zX^-$ species (X = $CO_2$ and $2CO_2$) are labeled as $x$,$y$,$z$ and +X, respectively.

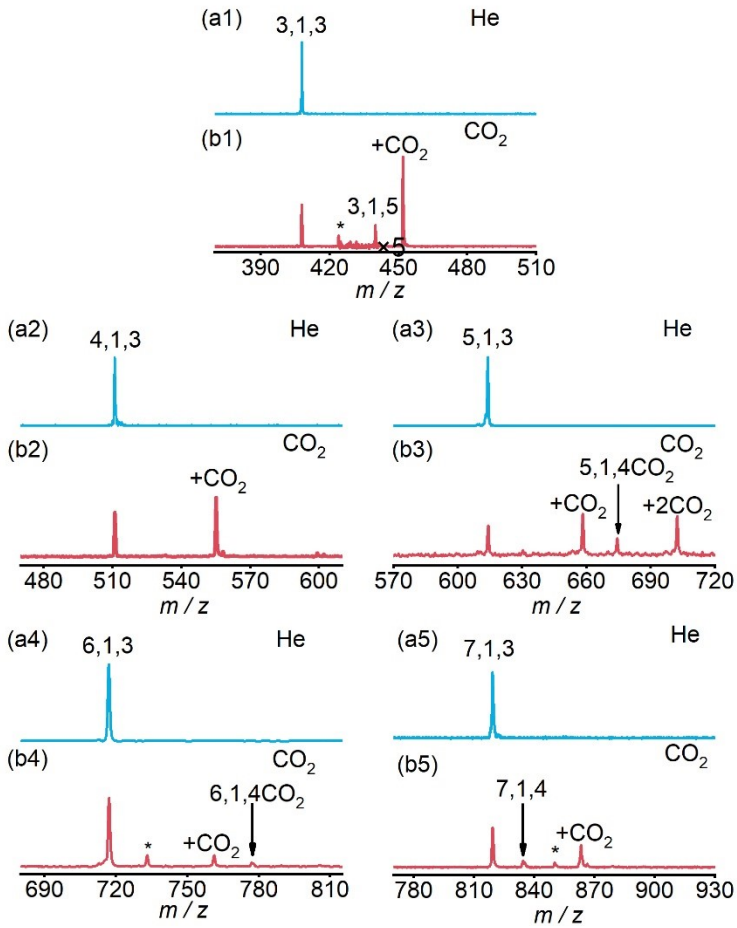


**Fig. S4** The TOF mass spectra for the reactions of mass-selected $Rh_nVO_3^-$ ($n$ = 3–7) clusters (a) with $CO_2$ (b) at 573 K. The average molecule density of reactant gas is about 18 × $10^{12}$ (b1), 92× $10^{12}$ (b2), 326 × $10^{12}$ (b3), 114 × $10^{12}$ (b4), and 17 × $10^{12}$ molecule per $cm^3$ (b5). The reaction times are about 1.7 ms for $Rh_{3\text{-}5}VO_3^-$ + $CO_2$, 22.0 ms for $Rh_6VO_3^-$ + $CO_2$ and 1.8 ms for $Rh_7VO_3^-$ + $CO_2$. The $Rh_xV_yO_z^-$ and $Rh_xV_yO_zX^-$ species (X = $CO_2$ and $2CO_2$) are labeled as $x$,$y$,$z$ and +X, respectively. The peaks marked as asterisks are $Rh_3VO_4^-$ (b1), $Rh_6VO_4^-$ (b4) and $Rh_7VO_5^-$ (b5), respectively.

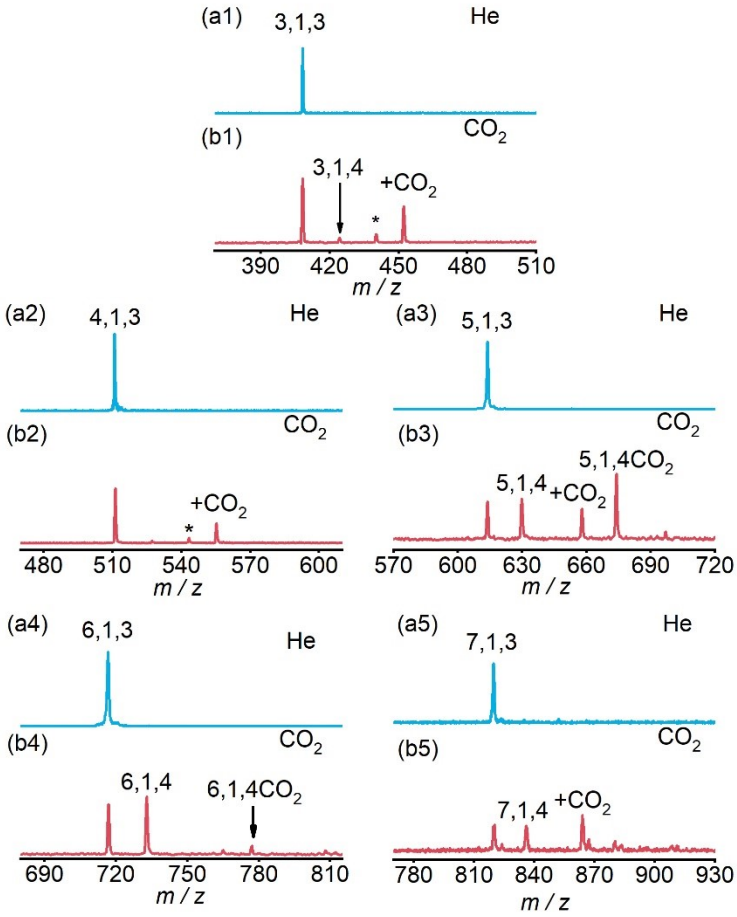


**Fig. S5** The TOF mass spectra for the reactions of mass-selected $Rh_nVO_3^-$ ($n$ = 3–7) clusters (a) with $CO_2$ (b) at 673 K. The average molecule density of reactant gas is about 17 × $10^{12}$ (b1), 7× $10^{12}$ (b2), 18 × $10^{12}$ (b3), 153 × $10^{12}$ (b4), and 74 × $10^{12}$ molecule per $cm^3$ (b5). The reaction times are about 2.0 ms for $Rh_{3,7}VO_3^-$ + $CO_2$, 12.0 ms for $Rh_{4,5}VO_3^-$ + $CO_2$, and 42.0 ms for $Rh_6VO_3^-$ + $CO_2$. The $Rh_xV_yO_z^-$ and $Rh_xV_yO_zX^-$ species (X = $CO_2$ and $2CO_2$) are labeled as $x$,$y$,$z$ and +X, respectively. The peaks marked as asterisks are $Rh_3VO_5^-$ (b1) and $Rh_4VO_5^-$ (b2) respectively.

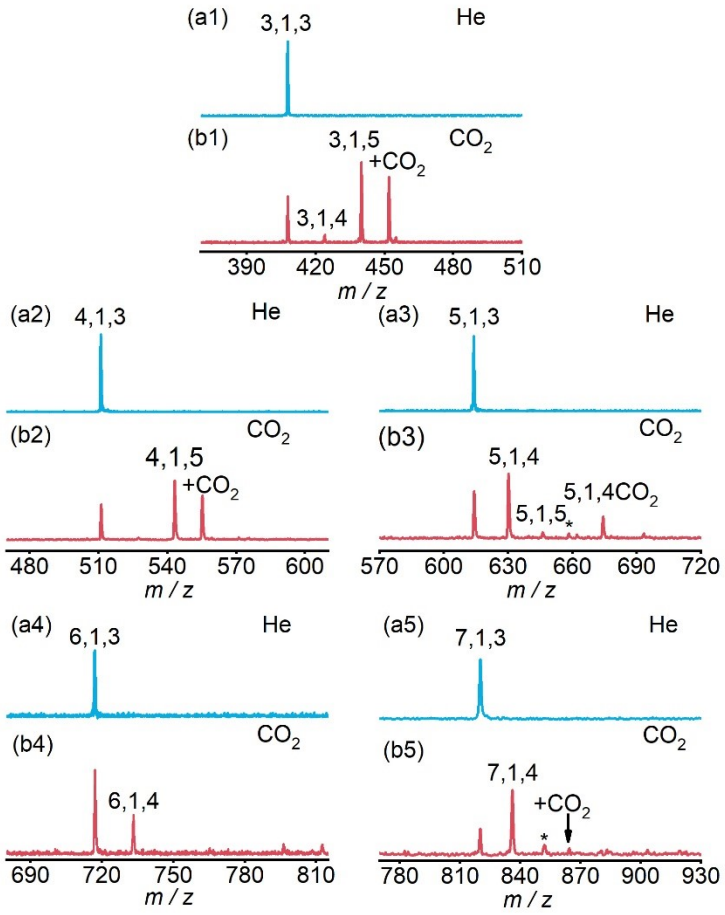


**Fig. S6** The TOF mass spectra for the reactions of mass-selected $Rh_nVO_3^-$ ($n$ = 3–7) clusters (a) with $CO_2$ (b) at 773 K. The average molecule density of reactant gas is about 22 × $10^{12}$ (b1), 130× $10^{12}$ (b2), 129 × $10^{12}$ (b3), 78 × $10^{12}$ (b4), and 65 × $10^{12}$ molecule per $cm^3$ (b5). The reaction times are about 2.0 ms for $Rh_3VO_3^-$ + $CO_2$, 9.0 ms for $Rh_4VO_3^-$ + $CO_2$, 7.0 ms for $Rh_5VO_3^-$ + $CO_2$, 18.0 ms for $Rh_6VO_3^-$ + $CO_2$, 12.0 ms for $Rh_7VO_3^-$ + $CO_2$. The $Rh_xV_yO_z^-$ and $Rh_xV_yO_zX^-$ species (X = $CO_2$ and $2CO_2$) are labeled as $x$,$y$,$z$ and +X, respectively. The peak marked as asterisks are $Rh_5VO_3CO_2^-$ (b3) $Rh_7VO_5^-$ (b5).

## 2.2 Mass spectra for the reactions of mass-selected $Rh_nVO_4^-$ ($n$ = 3–7) clusters with $H_2$ at variable temperatures (298 – 673K)

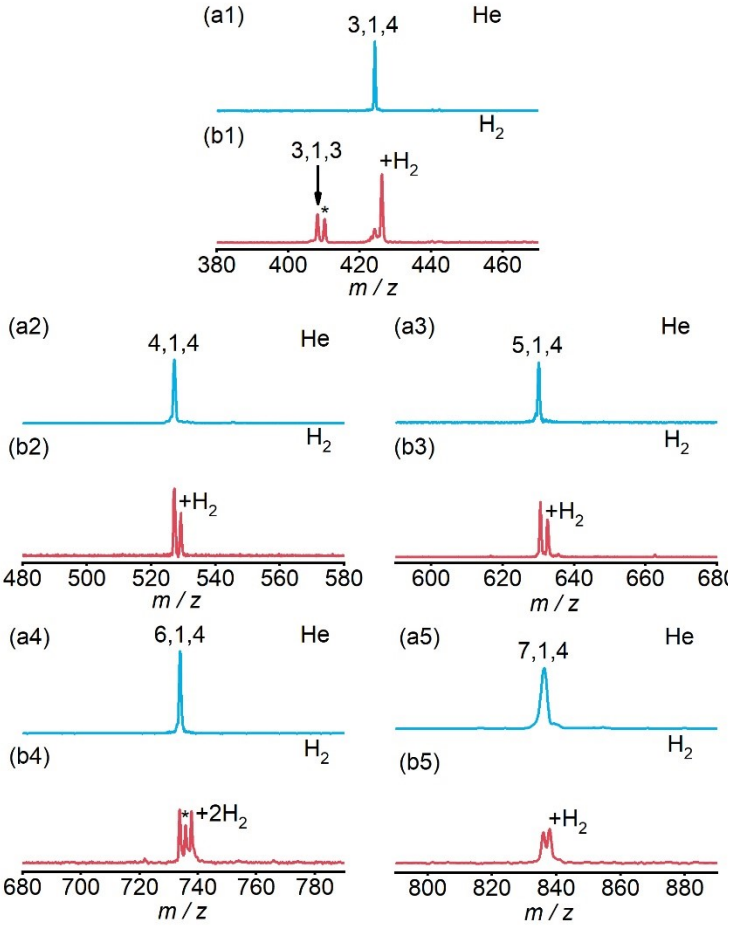


**Fig. S7** The TOF mass spectra for the reactions of mass-selected $Rh_nVO_4^-$ ($n$ = 3–7) clusters (a) with $H_2$ (b) at 298 K. The average molecule density of reactant gas is about 11 × $10^{12}$ (b1), 8× $10^{12}$ (b2), 5 × $10^{12}$ (b3), 21 × $10^{12}$ (b4), and 8 × $10^{12}$ molecule per $cm^3$ (b5). The reaction times are about 1.0 ms for $Rh_{3,4}VO_4^-$ + $H_2$, 2.0 ms for $Rh_{5\text{-}7}VO_4^-$ + $H_2$. The $Rh_xV_yO_z^-$ and $Rh_xV_yO_zX^-$ species (X = $H_2$ and $2H_2$) are labeled as $x$,$y$,$z$ and +X, respectively. The peaks marked as asterisks are $Rh_3VO_3H_2^-$ (b1) and $Rh_6VO_4H_2^-$ (b4), respectively.

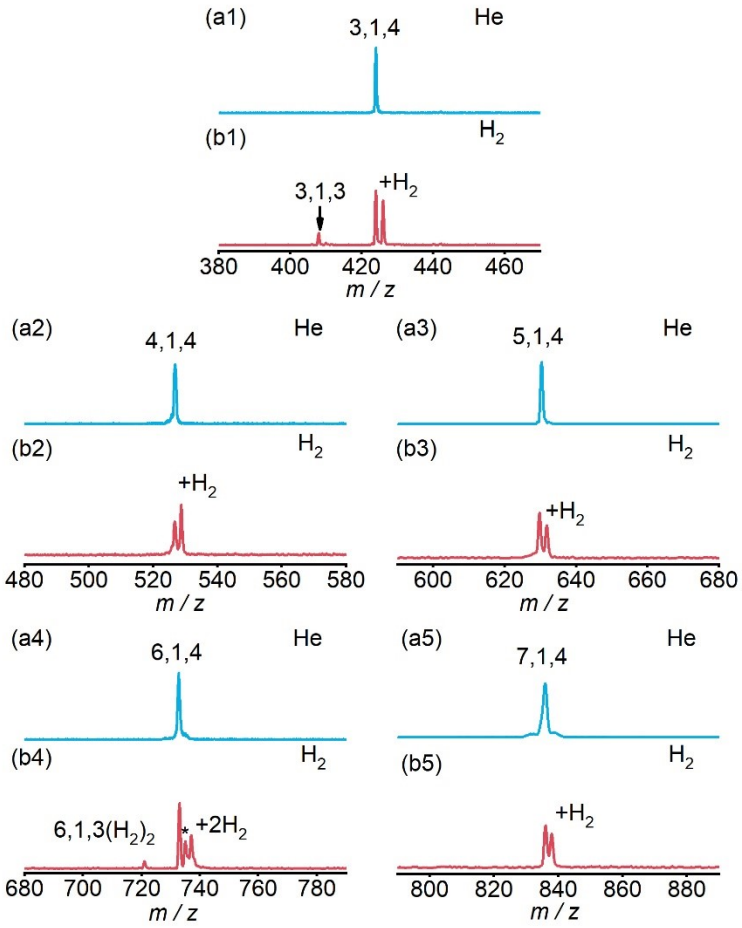


**Fig. S8** The TOF mass spectra for the reactions of mass-selected $Rh_nVO_4^-$ ($n$ = 3–7) clusters (a) with $H_2$ (b) at 373 K. The average molecule density of reactant gas is about 4 × $10^{12}$ (b1), 4× $10^{12}$ (b2), 17 × $10^{12}$ (b3), 56× $10^{12}$ (b4), and 7 × $10^{12}$ molecule per $cm^3$ (b5). The reaction times are about 1.7 ms for $Rh_{3,5}VO_4^-$ + $H_2$, 1.8 ms for $Rh_4VO_4^-$ + $H_2$, 2.1 ms for $Rh_6VO_4^-$ + $H_2$, 1.9 ms for $Rh_7VO_4^-$ + $H_2$. The $Rh_xV_yO_z^-$ and $Rh_xV_yO_zX^-$ species (X = $H_2$ and $2H_2$) are labeled as $x$,$y$,$z$ and +X, respectively. The peak marked as asterisk is $Rh_6VO_4H_2^-$ (b4).

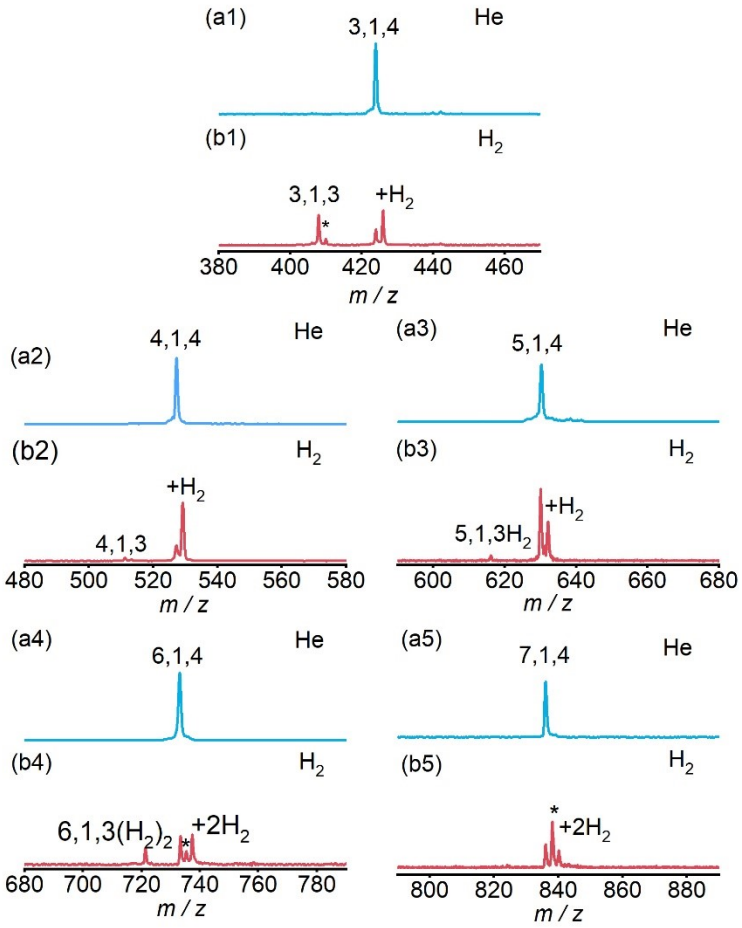


**Fig. S9** The TOF mass spectra for the reactions of mass-selected $Rh_nVO_4^-$ ($n$ = 3–7) clusters (a) with $H_2$ (b) at 473 K. The average molecule density of reactant gas is about 5 × $10^{12}$ (b1), 15× $10^{12}$ (b2), 18 × $10^{12}$ (b3), 53× $10^{12}$ (b4), and 44 × $10^{12}$ molecule per $cm^3$ (b5). The reaction times are about 1.7 ms for $Rh_3VO_4^-$ + $H_2$, 2.0 ms for $Rh_{4,5}VO_4^-$ + $H_2$, 12.0 ms for $Rh_6VO_4^-$ + $H_2$, 1.9 ms for $Rh_7VO_4^-$ + $H_2$. The $Rh_xV_yO_z^-$ and $Rh_xV_yO_zX^-$ species (X = $H_2$ and $2H_2$) are labeled as $x$,$y$,$z$ and +X, respectively. The peaks marked as asterisks are $Rh_3VO_3H_2^-$ (b1) $Rh_6VO_4H_2^-$ (b4) and $Rh_7VO_4H_2^-$ (b5), respectively.

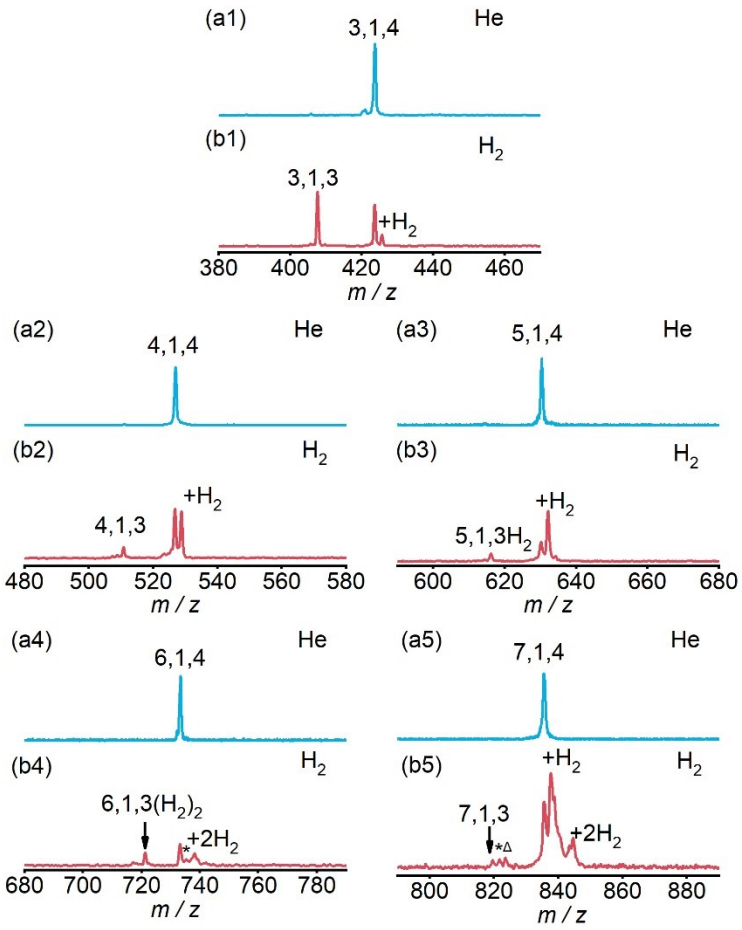


**Fig. S10** The TOF mass spectra for the reactions of mass-selected $Rh_nVO_4^-$ ($n$ = 3–7) clusters (a) with $H_2$ (b) at 573 K. The average molecule density of reactant gas is about 4 × $10^{12}$ (b1), 16× $10^{12}$ (b2), 67 × $10^{12}$ (b3), 1193 × $10^{12}$ (b4), and 197 × $10^{12}$ molecule per $cm^3$ (b5). The reaction times are about 1.7 ms for $Rh_{3\text{-}5}VO_4^-$ + $H_2$, 2.0 ms for $Rh_6VO_4^-$ + $H_2$, 1.8 ms for $Rh_7VO_4^-$ + $H_2$. The $Rh_xV_yO_z^-$ and $Rh_xV_yO_zX^-$ species (X = $H_2$ and $2H_2$) are labeled as $x$,$y$,$z$ and +X, respectively. The peaks marked as asterisks are $Rh_6VO_4H_2^-$ (b4) and $Rh_7VO_4H_2^-$ (b5) respectively. The peak marked as a triangle is $Rh_7VO_3(H_2)_2^-$.

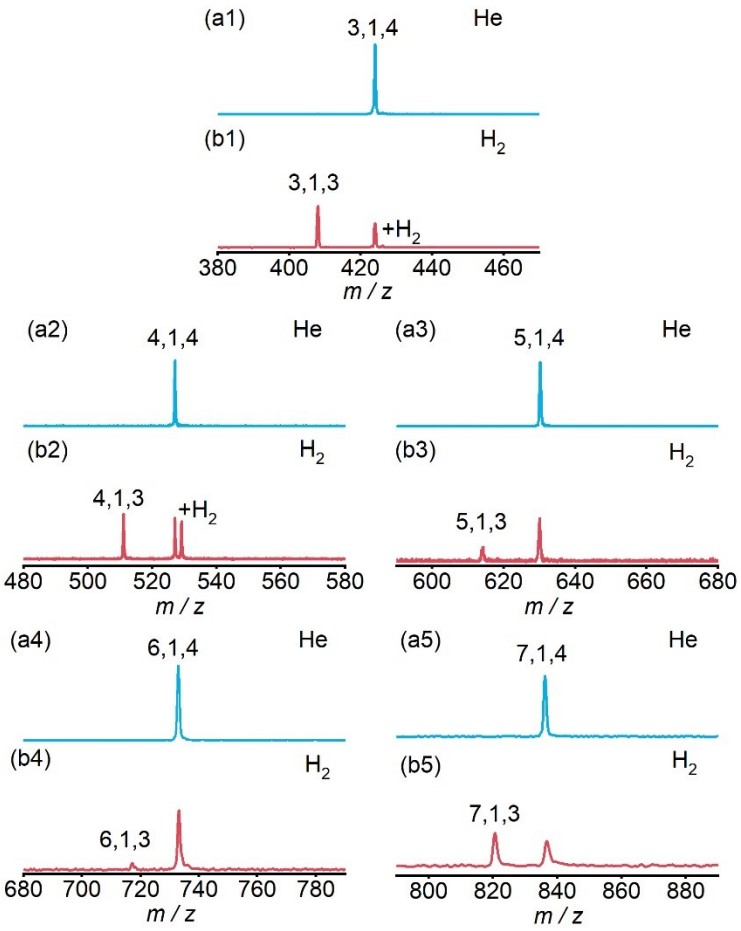


**Fig. S11** The TOF mass spectra for the reactions of mass-selected $Rh_nVO_4^-$ ($n$ = 3–7) clusters (a) with $H_2$ (b) at 673 K. The average molecule density of reactant gas is about 7 × $10^{12}$ (b1), 31 × $10^{12}$ (b2), 24 × $10^{12}$ (b3), 88 × $10^{12}$ (b4), and 53 × $10^{12}$ molecule per $cm^3$ (b5). The reaction times are about 1.9 ms for $Rh_{3,4}VO_4^-$ + $H_2$, 12.0 ms for $Rh_{5\text{-}7}VO_4^-$ + $H_2$. The $Rh_xV_yO_z^-$ and $Rh_xV_yO_zX^-$ species (X = $H_2$ and $2H_2$) are labeled as $x$,$y$,$z$ and +X, respectively.

## 2.3 The branching ratio of products $Rh_n^-$ for reactions $Rh_nO^-$ ($n$ = 3–7) + $H_2$ and $Rh_nVO_3^-$ for reactions $Rh_nVO_4^-$ + $H_2$ under variable temperatures (298 – 673K)

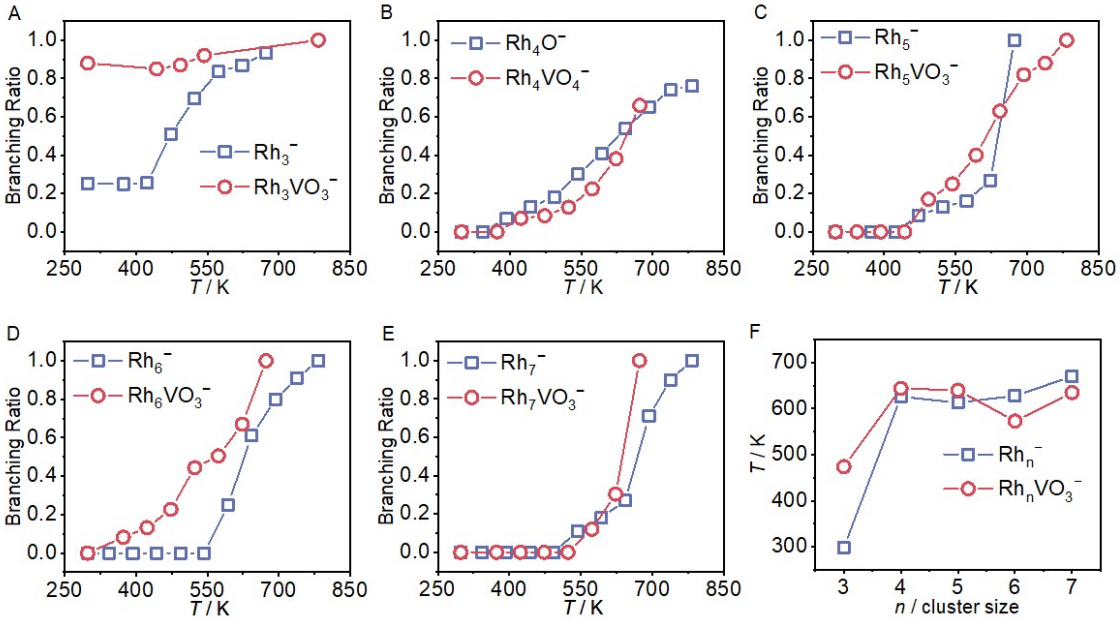


**Fig. S12** The branching ratio of products $Rh_n^-$ for reactions $Rh_nO^-$ ($n$ = 3–7) + $H_2$ and $Rh_nVO_3^-$ for reactions $Rh_nVO_4^-$ + $H_2$ under variable temperatures (A–E). Temperatures required when the abundance of products $Rh_n^-$ and $Rh_nVO_3^-$ reach the conversion of 50% (F).

## 3. Additional theoretical calculation results

### 3.1 Low-lying isomers of $Rh_nVO_3^-$ ($n$ = 3–7)

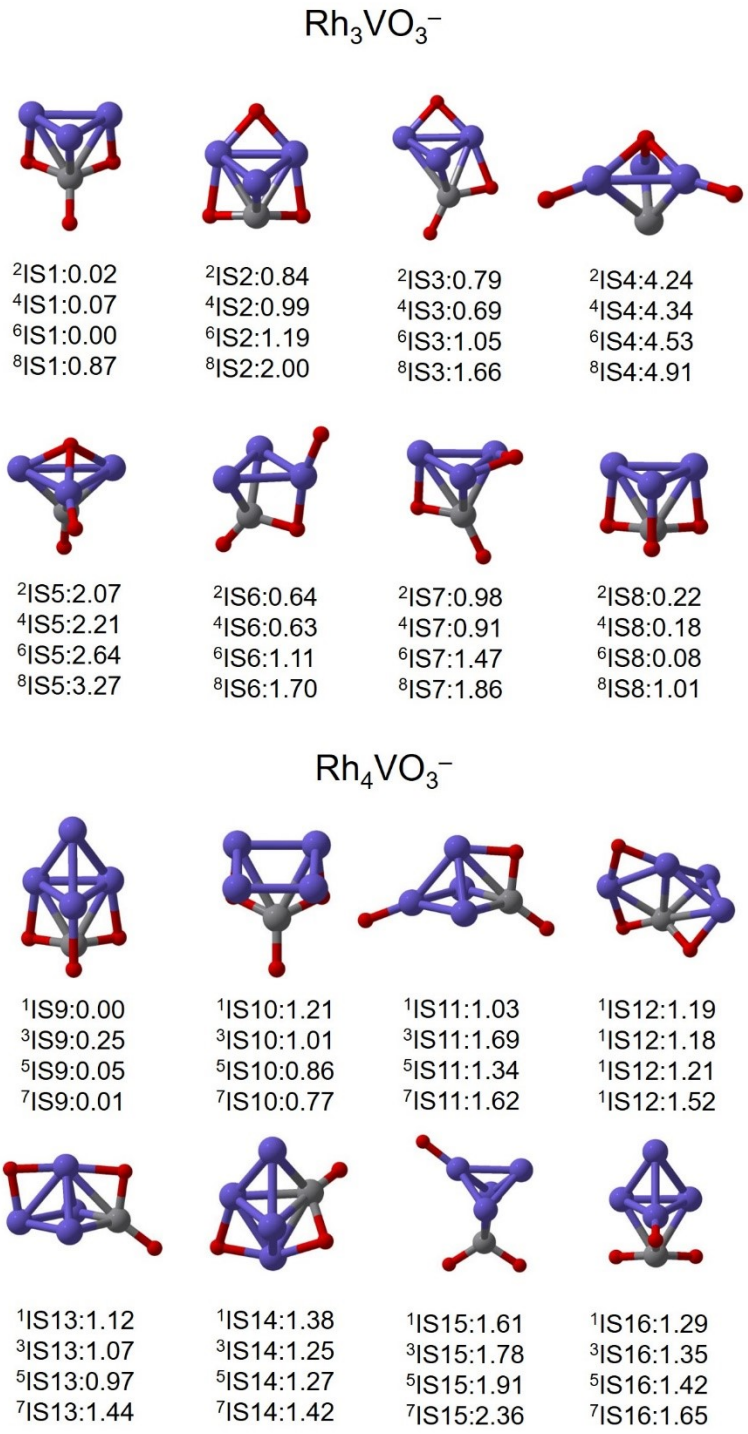


**Fig. S13** The DFT-calculated isomers for $Rh_{3,4}VO_3^-$ at the TPSS level. The relative energies with respect to the lowest-lying isomer are given in eV. Superscripts represent different spin multiplicities.

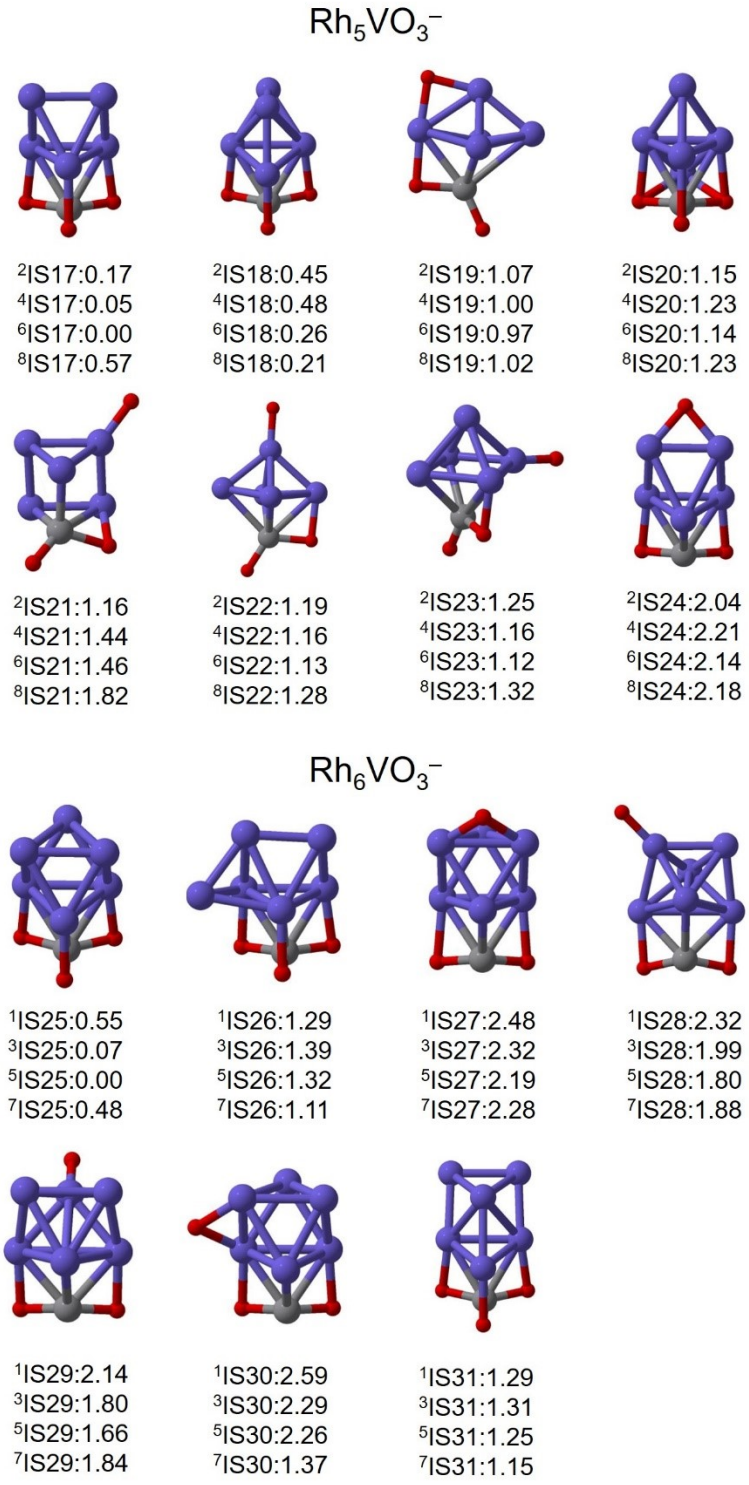


**Fig. S14** The DFT-calculated isomers for $Rh_{5,6}VO_3^-$ at the TPSS level. The relative energies with respect to the lowest-lying isomer are given in eV. Superscripts represent different spin multiplicities.

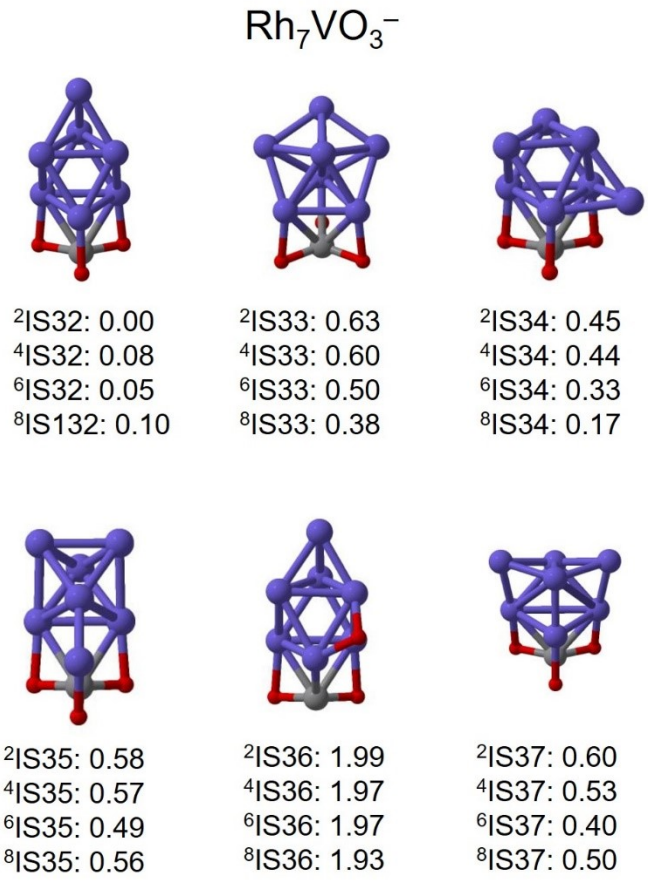


**Fig. S15** The DFT-calculated isomers for $Rh_7VO_3^-$ at the TPSS level. The relative energies with respect to the lowest-lying isomer are given in eV. Superscripts represent different spin multiplicities.

### 3.2 Low-lying isomers of $Rh_nVO_4^-$ ($n$ = 3–7)

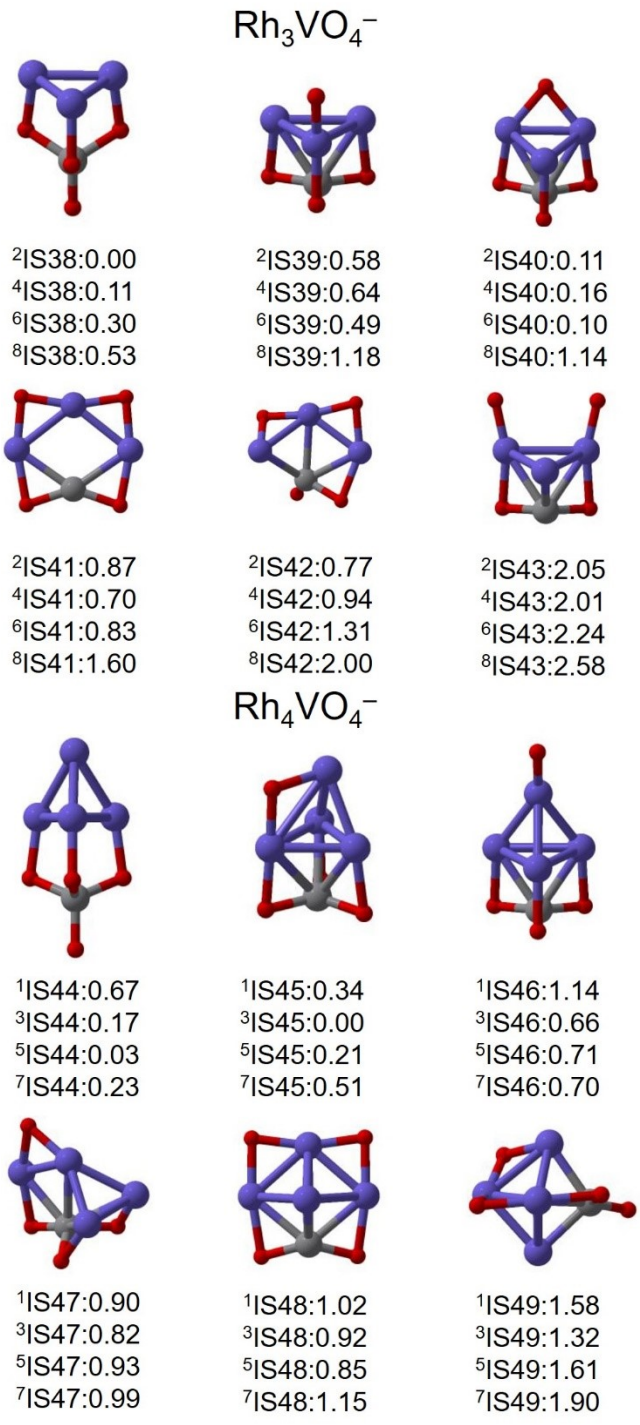


**Fig. S16** The DFT-calculated isomers for $Rh_{3,4}VO_4^-$ at the TPSS level. The relative energies with respect to the lowest-lying isomer are given in eV. Superscripts represent different spin multiplicities.

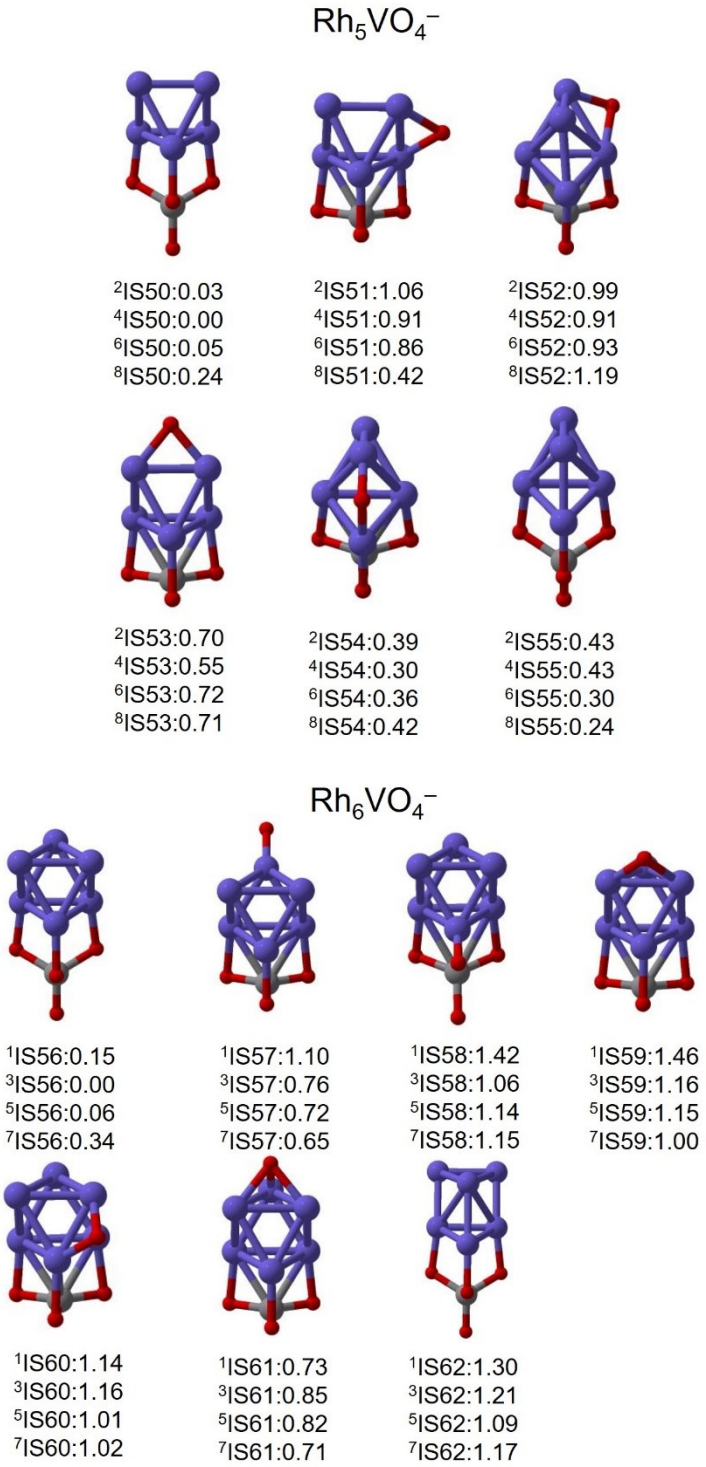


**Fig. S17** The DFT-calculated isomers for $Rh_{5,6}VO_4^-$ at the TPSS level. The relative energies with respect to the lowest-lying isomer are given in eV. Superscripts represent different spin multiplicities.

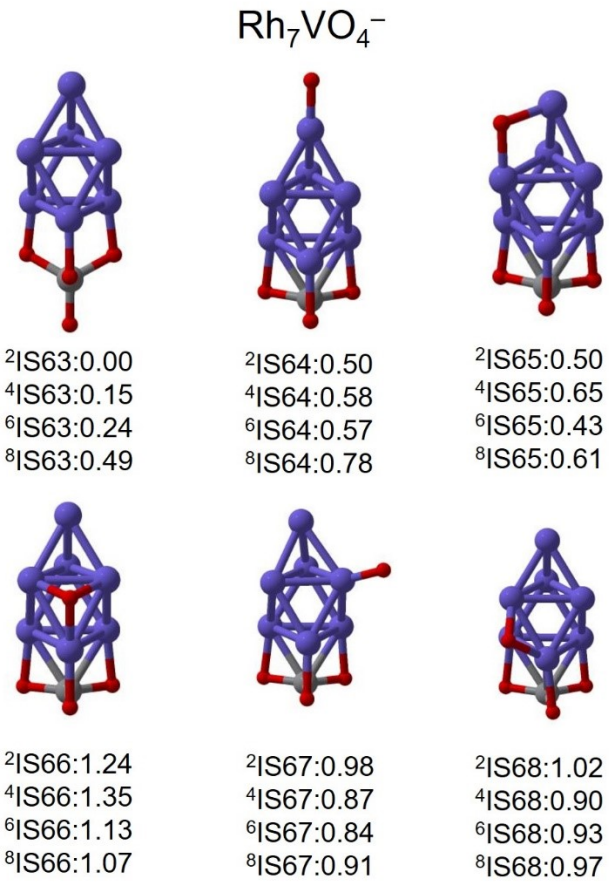


**Fig. S18** The DFT-calculated isomers for $Rh_7VO_4^-$ at the TPSS level. The relative energies with respect to the lowest-lying isomer are given in eV. Superscripts represent different spin multiplicities.

### 3.3 The DFT-calculated potential profile for $^5Rh_6VO_3^- + CO_2$

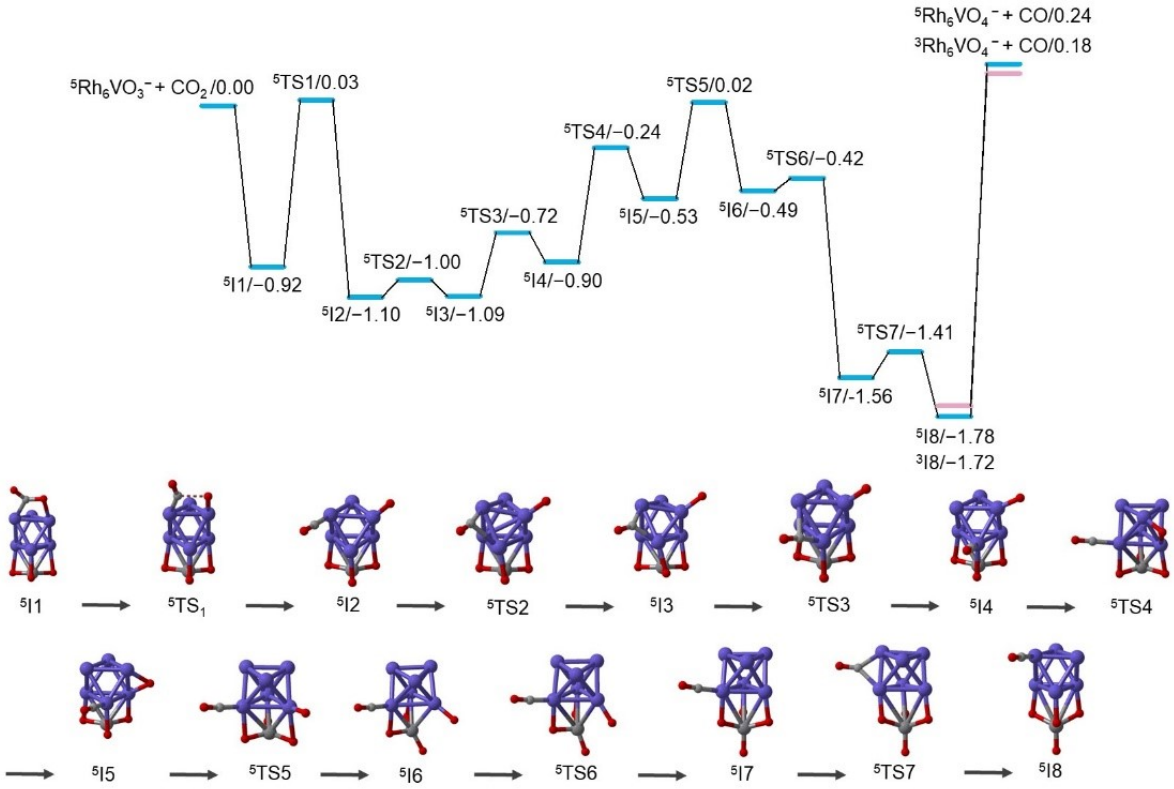


**Fig. S19** The DFT-calculated potential profile for $^5Rh_6VO_3^- + CO_2$. The zero-point-vibration-corrected energies ($\Delta H_0$, eV) with respect to the separated reactants are given in eV. The superscripts represent the spin multiplicities.

## 4. References


1. W.-G. Wang, Z.-C.Wang, S. Yin, S.-G. He and M.-F. Ge, *Chin. J. Chem. Phys.*, 2007, **20**, 412–418.
2. X.-N. Wu, B. Xu, J.-H. Meng and S.-G. He, *Int. J. Mass. Spectrom.*, 2012, **310**, 57–64.
3. X.-N. Wu, Y.-X. Zhao, W. Xue, Z.-C. Wang, S.-G. He and X.-L. Ding, *Phys. Chem. Chem. Phys.*, 2010, **12**, 3984–3997.
4. W. Xue, S. Yin, X.-L. Ding, S.-G. He and M.-F. Ge, *J. Phys. Chem. A*, 2009, **113**, 5302–5309.
5. Z. Yuan, Z.-Y. Li, Z.-X. Zhou, Q.-Y. Liu, Y.-X. Zhao and S.-G. He, *J. Phys. Chem. C*, 2014, **118**, 14967–14976.
6. M. Ruan, Q.-Y. Liu, Y.-X. Zhao, G.-P. Wei, X.-G. Zhao, Q. Li and S.-G. He, *J. Chem. Phys.*, 2022, **157**, 114301.
7. L.-X. Jiang, Q.-Y. Liu, X.-N. Li and S.-G. He, *J. Am. Soc. Mass. Spectr.*, 2018, **29**, 78–84.
8. J. Tao, J. P. Perdew, V. N. Staroverov and G. E. Scuseria, *Phys. Rev. Lett.*, 2003, **91**, 146401.
9. M. J. Frisch, G. W. Trucks, H. B. Schlegel, G. E. Scuseria, M. A. Robb, J. R. Cheeseman, G. Scalmani, V. Barone, B. Mennucci, G. A. Petersson, H. Nakatsuji, M. Caricato, X. Li, H. P. Hratchian, A. F. Izmaylov, J. Bloino, G. Zheng, J. L. Sonnenberg, M. Hada, M. Ehara, K. Toyota, R. Fukuda, J. Hasegawa, M. Ishida, T. Nakajima, Y. Honda, O. Kitao, H. Nakai, T. Vreven, J. A. Montgomery, Jr., J. E. Peralta, F. Ogliaro, M. Bearpark, J. J. Heyd, E. Brothers, K. N. Kudin, V. N. Staroverov, R. Kobayashi, J. Normand, K. Raghavachari, A. Rendell, J. C. Burant, S. S. Iyengar, J. Tomasi, M. Cossi, N. Rega, J. M. Millam, M. Klene, J. E. Knox, J. B. Cross, V. Bakken, C. Adamo, J. Jaramillo, R. Gomperts, R. E. Stratmann, O. Yazyev, A. J. Austin, R. Cammi, C. Pomelli, J. W. Ochterski, R. L. Martin, K. Morokuma, V. G. Zakrzewski, G. A. Voth, P. Salvador, J. J. Dannenberg, S. Dapprich, A. D. Daniels, O. Farkas, J. B. Foresman, J. V. Ortiz, J. Cioslowski and D. J. Fox. *Gaussian 09 Revision A.01.,* 2009.
10. A. Schäfer, C. Huber and R. Ahlrichs, *J. Chem. Phys.*, 1994, **100**, 5829–5835.
11. D. Andrae, U. Häußermann, M. Dolg, H. Stoll and H. Preuß, *Theor. Chim. Acta*, 1990, **77**, 123–141.
12. X.-L. Ding, Z.-Y. Li, J.-H. Meng, Y.-X. Zhao and S.-G. He, *J. Chem. Phys.*, 2012, **137**, 214311.
13. H. B. Schlegel, *J. Comput. Chem.*, 1982, **3**, 214–218.
14. C. Gonzalez and H. B. Schlegel, *J. Chem. Phys.*, 1989, **90**, 2154–2161.
15. E. D. Glendening, J. K. Badenhoop, A. E. Reed, J. E. Carpenter, J. A. M. Bohmann, C. M. and F. Weinhold., 2012. http://www.chem.wisc.edu/.